Superresolution effect due to a thin dielectric slab for imaging with radially polarized light

Meng, Peiwen; Pereira, S. F.; Dou, Xiujie; Urbach, H. P.

DOI
10.1364/OE.390602

Publication date
2020

Document Version
Final published version

Published in
Optics Express

Research Article | Vol. 28, No. 14 / 6 July 2020 / Optics Express 20660
Optics EXPRESS

Superresolution effect due to a thin dielectric slab for imaging with radially polarized light

PEIWEN MENG,[1,*] S. F. PEREIRA,[1] XIUJIE DOU,[1,2] AND H. P. URBACH[1]

[1] Optics Research Group, Department of Imaging Physics, Delft University of Technology, Lorentzweg 1, 2628 CJ Delft, The Netherlands
[2] Nanophotonics Research Center, Shenzhen University, Shenzhen 518060, China
[*] p.meng@tudelft.nl

Abstract: Improving the image quality of small particles is a classic problem and especially challenging when the distance between particles are below the optical diffraction limit. We propose a imaging system illuminated with radially polarized light combined with a suitable substrate that contains a thin dielectric layer to demonstrate that the imaging quality can be enhanced. The coupling between the evanescent wave produced in a designed thin dielectric layer, the small particles and the propagating wave forms a mechanism to transfer sub-wavelength information about the particles to the far field. The smallest distinguished distance reaches to 0.634λ, when the imaging system is composed of a high numerical aperture (NA=0.9) lens and the illumination wavelength $\lambda = 632nm$, beyond the diffraction limit 0.678λ. The lateral resolution can be further improved by combining the proposed structure with superresolution microscopy techniques.

1. Introduction

The conventional optical microscopy with lenses and mirrors are naturally limited by diffraction to about half of the wavelength of the light [1]. The limit is due to the loss of high-resolution details from the near field to the far field. To overcome this limit, far-field microscopy techniques with super-resolution such as stochastic optical reconstruction microscopy (STORM) [2], photo activated localization microscopy (PALM) [3,4], stimulated emission depletion (STED) [5] and structured illumination microscopy (SIM) [6] have been developed. Although these superresolution tehcniques are attractive, disadvantages such as costs, time-consuming data acquisition and choices of fluorescent dyes limit their applications. In the case of confocal microscopes with laser, a sharp focal spot is important. One way to achieve this is focusing a radially polarized (RP) beam with a NA objective lens [7,8]. Combined with a ring mask, even a smaller focal spot can be obtained. In this case, better resolution of imaging two longitudinal dipoles is investigated theoretically [9].

In general, a substrate is necessary for supporting the sample on the microscope. A specially designed substrate containing a thin layer of some designed material and thickness on top of it can be helpful in improving the imaging quality. Veselago was the first to mention materials with negative refractive index [10]. Pendry demonstrated that besides focusing light, these materials would be able to enhance evanescent waves and lead to imaging beyond the diffraction limit [11]. Melville gave the experimental confirmation of super-resolution with a planar silver layer [12]. Although evanescent waves carry the information of high spatial frequency, they are confined to the near field and cannot contribute to the formation of final images. Far-field optical superlenses can significantly enhance the evanescent waves and convert them into propagating waves that can be measured in the far field [13,14]. It was found that a thin dielectric layer can restore evanescent waves as a silver lens does and realize super-resolution, with the advantage that it is easier to deposit thin layers without percolation issues observed for metals [15,16]. A simple but

#390602 https://doi.org/10.1364/OE.390602
Journal © 2020 Received 14 Feb 2020; revised 17 Apr 2020; accepted 11 May 2020; published 29 Jun 2020

Optics EXPRESS

complete system of evanescent-wave generation, amplification, and the consequent modulation of the far field was designed in [17]. The far field propagating waves containing information about sub-wavelength objects by coupling evanescent waves can be used in microscopy to recover sub-wavelength details.

In this paper, we investigate the effect of evanescent waves for imaging subwavelength particles on a flat substrate coated with a very thin evanescent wave amplifying layer. In the section of theoretical model, the model is built by considering the subwavelength particle as an electric dipole. It is demonstrated analytically that the evanescent wave can be enhanced in the near field compared with the case of no enhanced layers in the section of simulation results and discussion. Also, we use numerical analysis based on a three-dimensional (3D) finite difference time domain (FDTD) method to simulate the near field distributions when one or two nanospheres are taken into account. The images of the spheres are reconstructed using the methods of angular spectrum and Fourier transform. Through the calculations, far field imaging quality of both signal-to-noise ratio (SNR) and lateral resolution can be enhanced in a simple designed structure. Finally, it can be summarized that the results can be easily applied in other imaging systems, hence immediately improving their performance.

2. Theoretical model

The schematic diagram describing the complete imaging process is shown in Fig. 1(a). The radially polarized light is formed after the red light ($\lambda = 632nm$) passes through the polarization convertor. Then the light is tightly focused by a high NA=0.9 objective lens on a substrate. The information of the sample can be collected in the far field and finally recorded by the CCD. The complex interactions happen between the incident beam, the sample and the thin layer. In order to understand the interactions better, Fig. 1(b) gives a detailed illustration of the sample and explains the mechanism of enhancement of evanescent waves [17]. When the incident light (red arrows) illuminates the small particle, evanescent waves can be generated. The direct scattered light (green arrows) includes both propagating and evanescent waves. Some of the scattered light propagates to the far field, while others go into the substrate. The reflected light contains propagating and evanescent waves. In the thin layer, the evanescent wave can be enhanced [15]. After that, the particle can be re-excited by the propagating wave and enhanced evanescent wave. Finally, it will cause a new round of scattering (yellow arrows) to the far field. Compared with the case of no enhanced layer, the evanescent wave decays very quickly in the substrate and cannot interacts with the particle. However, by adding a specially designed thin layer, the particle can be re-excited by the increased evanescent waves and new propagating waves can be produced, which provides more information in the far field.

To understand the principle of the whole imaging process mathematically, let us consider a Cartesian system (x, y, z) with z as the propagation direction. Since the particle here is subwavelength, it can be regarded as an electric dipole and Fig. 2 presents the schematic geometry of the problem. As it is known, the dyadic Green's function method [18] is widely used technique in solving problems involving dipole emission near planar surfaces. The field emitted by the dipole in the upper free space (z>0) can be written as the summation from two contributions [19]: [1] the emission of the dipole in free space described by the free space Green's function $\mathbf{G}_0$ and [2] the reflected field by the surface described by $\mathbf{G}_r$:

$$\mathbf{U}_{\text{dipole}}(\mathbf{r}) = (\mathbf{G}_0(\mathbf{r}, \mathbf{r}_\text{p}) + \mathbf{G}_r(\mathbf{r}, \mathbf{r}_\text{p}))\mathbf{p}, \tag{1}$$

where $\mathbf{r} = (x, y, z)$ is the position vector of the observation, and $\mathbf{r}_\text{p} = (x_\text{p}, y_\text{p}, z_\text{p})$ is the position vector of the dipole. The free space Green's function $\mathbf{G}_0$ is

$$\mathbf{G}_0(\mathbf{r}) = -\frac{1}{4\pi}\frac{e^{ik_0|\mathbf{r}-\mathbf{r}_\text{p}|}}{|\mathbf{r}-\mathbf{r}_\text{p}|}\frac{k_0^2}{\epsilon_0}, \tag{2}$$

Optics EXPRESS

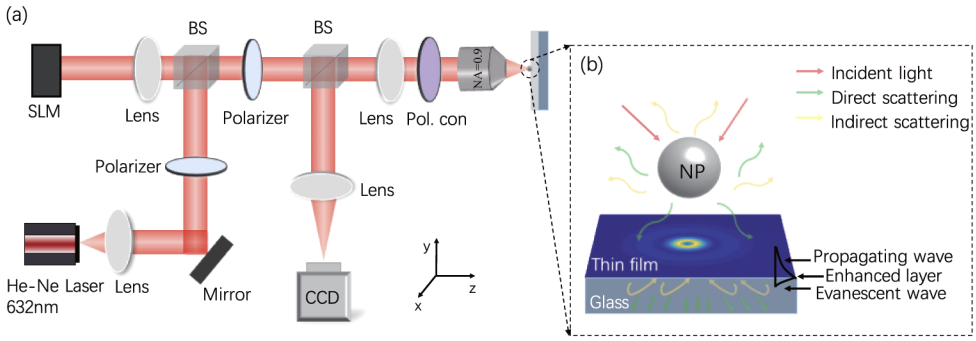

Fig. 1. Schematic diagram of the imaging system. (a) A complete imaging setup with the illumination of radially polarized beam at the wavelength $\lambda = 632nm$. (b) The mechanism of enhancement of evanescent waves by considering a sample on the glass substrate with a thin dielectric film on the top. Abbreviations: beam splitter (BS), spatial light modulator (SLM), polarization convertor (Pol.con), nanoparticle (NP).

here ϵ_0 is the permittivity of the free space.

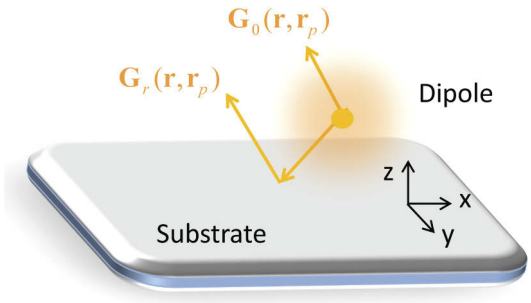

Fig. 2. Schematic geometry of a dipole placed above the substrate.

$\mathbf{p}$ represents the dipole moment, and we assume it is known and is expressed as

$$\mathbf{p} = \alpha \mathbf{U}_{\text{tot}}^{in}(\mathbf{r}_\text{p}) + \alpha \mathbf{G}_r(\mathbf{r}, \mathbf{r}_\text{p})\mathbf{p}, \tag{3}$$

It is seen that the reflected field modifies the dipole moment and the effect is called the Purcell effect. If the polarizability α is known, so that

$$\mathbf{p} = \frac{\alpha \mathbf{U}_{\text{tot}}^{in}(\mathbf{r}_\text{p})}{1 - \alpha \mathbf{G}_r(\mathbf{r}, \mathbf{r}_\text{p})}, \tag{4}$$

where $\mathbf{U}_{\text{tot}}^{in}$ is related to the total incident field. The reflective field is the inverse Fourier transform of the reflection coefficient times the Fourier transform of the field in homogeneous space and a phase factor due to propagation from z_p to z. The reflective Green's function $\mathbf{G}_r$ is

$$\mathbf{G}_{r(\mathbf{r}}, \mathbf{r}_\mathbf{p} = \frac{1}{4\pi^2} \iint \mathbf{R}(k_\perp) \mathscr{F}(\mathbf{G}_0) \left(\frac{k_x}{2\pi}, \frac{k_y}{2\pi}, z_p \right) e^{i[k_x(x-x_p)+k_y(y-y_p)+k_z z]} dk_x dk_y, \tag{5}$$

where

$$\mathscr{F}(\mathbf{G}_0(\mathbf{r}, \mathbf{r}_\text{p})) = \frac{e^{-i\left(k_x x_p + k_y y_p - k_z |z - z_p|\right)}}{2ik_z} dk_x dk_y, \tag{6}$$

Optics EXPRESS

where $\mathbf{k} = (k_x, k_y, k_z)$ is the wave vector, $\mathbf{k}_\perp = (k_x, k_y)$ is the part of the wave vector perpendicular to the optical axis, with $k_\perp = \sqrt{k_x^2 + k_y^2}$ its length, $k_z = \sqrt{k_0^2 n^2 - k_\perp^2}$, where $k_0 = 2\pi/\lambda_0$ is the wave number in free space and λ_0 is the wavelength in vacuum. $\mathbf{R}$ and $\mathscr{F}$ denote as the reflective coefficient and the operation of Fourier transform, respectively.

The Fresnel reflection coefficient for a wave incident from a medium with refractive index n_i on an interface of a medium with refractive index n_j is:

$$r_{i,j} = \frac{k_{z,i} - k_{z,j}}{k_{z,i} + k_{z,j}}, \tag{7}$$

where $k_{z,j}$ is the z component of the wave vector in the material with refractive index n_i.

The reflective coefficient becomes

$$\mathbf{R}(k_\perp) = r_{1,2} + t_{2,1} r_{2,3} t_{1,2} e^{2ik_{z,2}d} \{1 + r_{2,3} r_{2,1} e^{2ik_{z,2}d} + \cdots\}, \tag{8}$$

where the Fresnel transmission coefficient $t_{i,j} = 1 + r_{i,j} = \frac{2k_{z,i}}{k_{z,i}+k_{z,j}}$.

As the Green's function can be calculated numerically with stratified media [20], and substituting Eqs. (2) and (5) into Eq. (1), the field radiated by the dipole $\mathbf{U}_{\text{dipole}}$ can be obtained. Next is the process of vectorial imaging [9], and on performing the matrix operations given in [21,22], the final imaging in the detector plane is expressed as

$$\mathbf{E}^{\text{img}} = \mathbf{R}_0^{-1} \cdot \mathbf{L}_2 \cdot \mathbf{L}_1^{-1} \cdot \mathbf{R}_0 \cdot \mathbf{U}_{\text{dipole}}, \tag{9}$$

where the matrix $\mathbf{R}_0$ describes the coordinate transformation for rotation round the z axis and the matrix $\mathbf{L}_n$ describes the changes in the electric field as in the lens, respectively:

$$\mathbf{R}_0 = \begin{bmatrix} \cos\phi & \sin\phi & 0 \\ -\sin\phi & \cos\phi & 0 \\ 0 & 0 & 1 \end{bmatrix}, \tag{10}$$

$$\mathbf{L}_n = \begin{bmatrix} \cos\theta_n & 0 & \sin\theta_n \\ 0 & 1 & 0 \\ -\sin\theta_n & 0 & \cos\theta_n \end{bmatrix}, \tag{11}$$

The subscript n indicates the effect of the objective lens 1 with the high NA, or that of the detector lens 2 with NA=0.3 in our model. The angle of θ_n denotes the tangential angle with respect to the z axis, while ϕ denotes the azimuthal angle with respect to the x axis.

The above calculations on the basis of the dipole approximation make the physical interaction between the illumination, particles, thin layer and substrate more easily to understand. However, in order to make the calculations more realist, one should consider real nanospheres as objects. Here, we perform numerical simulations using the FDTD method to obtain the near field in the case of finite size spheres. The images can be rebuilt with Eq. (9) by taking the simulated near field as $\mathrm{U}_{\text{dipole}}$.

3. Simulation results and discussion

3.1. Reflection coefficient

To validate the enhancement of the evanescent wave due to the thin layer added on top of the substrate, three kinds of interfaces are taken into account in the calculation: a thick glass

Optics EXPRESS

(n_{glass} = 1.5) substrate without enhanced layer, 20nm thin layer of TiO_2 (n_{TiO_2} = 2.3897) on top of the thick glass substrate, and 20nm thin layer of InSb (n_{InSb} = 4.2842 + 1.8107i) on top of the thick glass substrate. In Fig. 3, we plot the enhancement of the reflection coefficient (r>1) when the system is excited by evanescent wave (k_x/k_0>1). For the s polarized light in Fig. 3(a), the enhancement of the case with TiO_2 is much larger than that with InSb slab. The peak amplification happens at k_x/k_0 = 1.499, which is 4.606 times higher than the structure without the enhancement film. Similar phenomenon can be seen in Fig. 3(b) for the illumination of the p polarized light. In this case, with the thin InSb film, the enhancement starts from k_x/k_0>1, while with the TiO_2, the enhancement starts from k_x/k_0>1.281. Note that, the difference in the reflection coefficient for the two enhancing layers is smaller with the p polarized excitation, compared with the s polarized case. The results in Fig. 3 illustrate that the design of the thin film can amplify the evanescent wave in the near field, this does not occur when only a thick glass substrate is used.

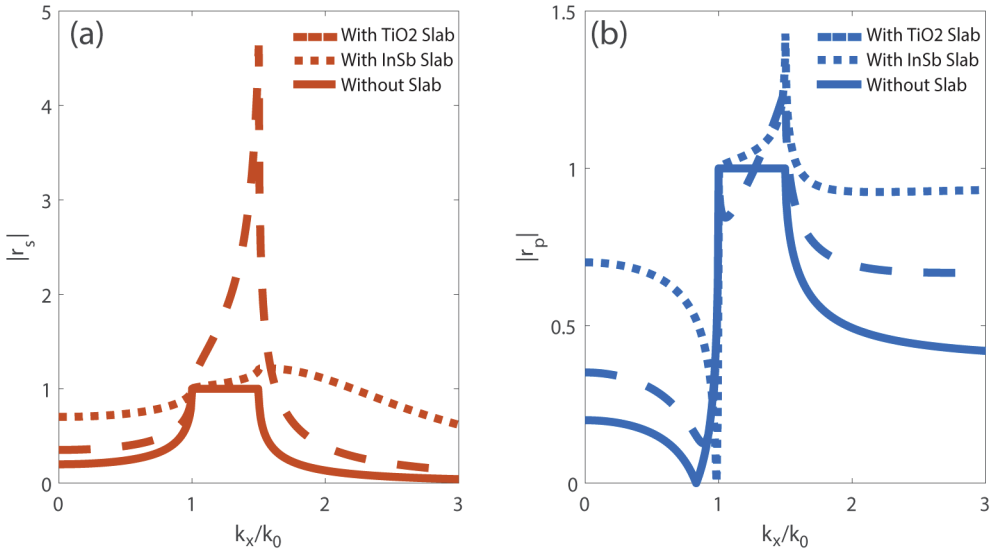

Fig. 3. The comparison on the modulus of the reflection coefficient for s (a) and p (b) polarized light at the interface of air and three kinds of substrates: without enhanced slab (solid line), with TiO_2 slab (dashed line) and with InSb slab (dot line) on top of the glass substrate.

3.2. Near field

To analyse the problem more rigorously, we add a dielectric nanosphere with radius r = 200nm as a sample on the top of the three substrates. The material of the sphere is polystyrene latex (PSL). By using numerical analysis-Lumerical FDTD, the near field distributions in the xz plane under the excitation of focused radially polarized light with the wavelength λ = 632nm are shown in Fig. 4. Strong scattering field can be seen with the adding slabs TiO_2 and InSb when radially polarized light (Figs. 4(a)-(c)) is focused on the top of the sample. Although the near field is enhanced, the scattering light is mainly localized. This is because of the large longitudinal component contained in the tightly focused radially polarized light [7]. A dipole excited by a focused radially polarized beam, will radiate radially polarized waves. If the dipole is on a substrate, there will be the radially polarized reflected fields as well. Looking at the reflection coefficients shown in Fig. 3, one observes that the values of $|r_p|$ are largest in the case of the InSb slab, which explains the corresponding strongest near field distribution in Figs. 4(c) when the

Optics EXPRESS

sample is illuminated by the radially polarized light. The enhanced signal can be achieved by inserting the enhancing layer and this gives an explanation of the improved scattering in the far field.

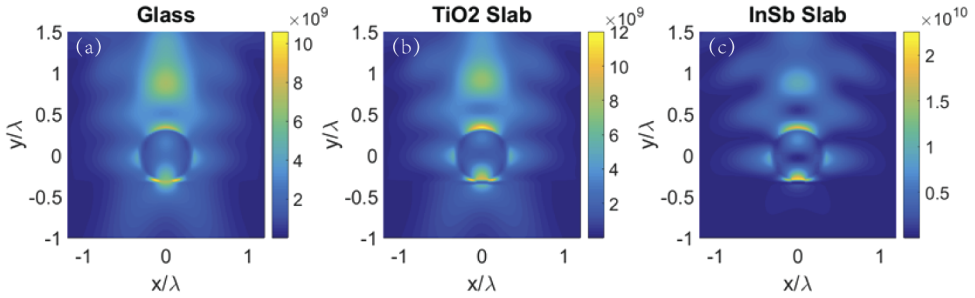

Fig. 4. The comparison of total intensity distributions in the near field of xz plane with the illumination radially polarized beams on the top of the nanosphere without (a), with TiO_2 (b) and with InSb (c) slab.

3.3. Imaging

Once the near fields are obtained, the final imaging can be calculated with Eqs. (9)–(11). The field of $\mathbf{U}_{\text{dipole}}$ is related to the near field above the top of the nanosphere in xy plane. Figure 5 displays the total scattering field distributions of one dielectric sphere in the xy imaging plane without (Fig. 5(a)) and with the enhancing layer (Figs. 5(b) and 5(c)) under the excitation of radially polarized beam. As the previous discussion, the total scattering fields are donut shaped. Comparing Figs. 5(b) and 5(c) with Fig. 5(a), it can be seen that when thin slabs are inserted, the SNR in the imaging plane are higher than the case of no enhanced layer. This agrees well with the results of near field distributions shown in Fig. 4. The corresponding cross section of the normalized total scattering fields is presented in Fig. 5(d). Even though the highest SNR is achieved with the InSb as an enhancing layer, the side lobes here are stronger than the case without the enhancing layer and with the layer of TiO_2. The side lobes will decrease the lateral resolution if more spheres are present in the neighborhood. Besides, the sharper distribution in the case of the TiO_2 thin layer, the more accurate particle localization [19]. This will be further demonstrated by the following discussion of imaging two particles.

In order to see whether the lateral resolution in the imaging plane can be improved or not, two identical nanospheres are considered as the new sample. The characteristics of the nanospheres are the same as that in Fig. 5. The two nanospheres are placed symmetrically with the y axis and the distance between them changes from $600nm$ to the smallest resolved value. Based on the performance of the high intensity and better localization in Fig. 5, we discuss the imaging of two spheres on the substrate with the enhancing TiO_2 layer is shown in Figs. 6(a_1)–6(d_1). For comparison, the imaging of two spheres on the substrate without the enhancing layer is shown in Figs. 6(a_2)–6(d_2). When the two spheres are separation by a large distance $600nm$, they can be resolved easily in both conditions. With the decrease of the separated distance, the resolved ability decreases as well. Similar to the Rayleigh criterion, it can be found that two spheres can still be distinguished with a distance of $d = 400nm$ in the case of with the enhancing TiO_2 layer, while they cannot be resolved anymore at the same distance without the enhancing layer. When the distance is down to $200nm$, the two particles are not distinguished anymore for both substrate cases. According to the Abbe diffraction limit $d = 0.61\lambda/\text{NA}$, the smallest distance that can be resolved is $d = 0.678\lambda$ in our imaging system theoretically. However, due to the combination of focused radial polarization and the addition of the enhancement layers, the two nanospheres can still be resolved when the distance between them decreases to $d = 400nm = 0.634\lambda$, which beyond

Optics EXPRESS

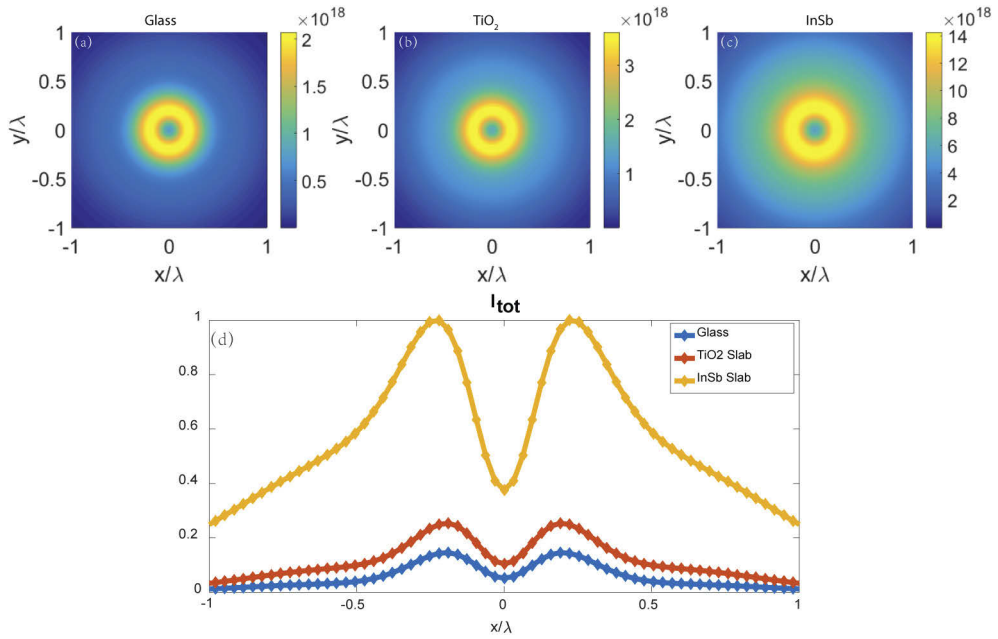

Fig. 5. Imaging of one sphere in the *xy* plane without (*a*) and with ((*b*)-TiO_2, (*c*)-InSb) the enhanced layer under the illumination of radially polarized light. (d) is the cross section of the normalized scattering intensity.

the diffraction limit and meaning improvement of the lateral resolution. Another important point to judge the imaging performance is the position of two spheres in the imaging plane. The center positions of the spheres in theory are given in red below each subplot and the corresponding positions in the imaging plane with and without the enhancing layer are marked in black dashed

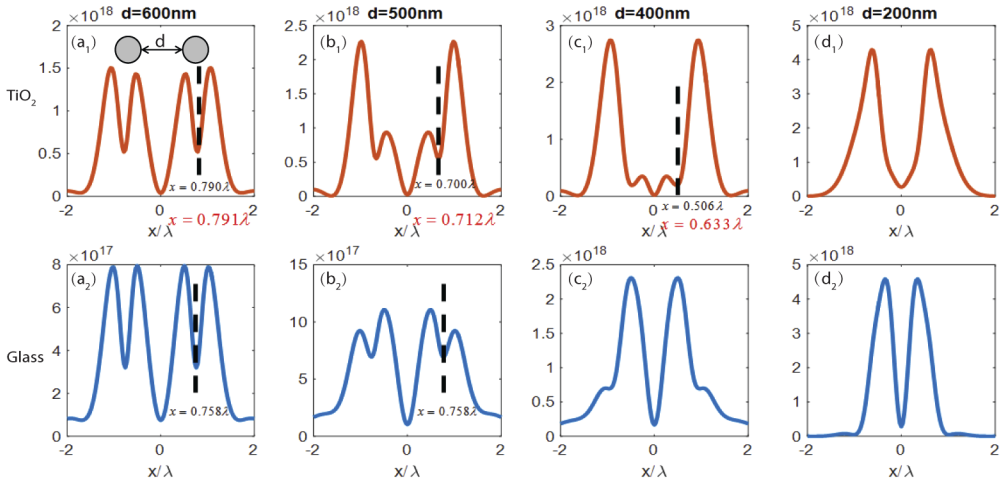

Fig. 6. Profile of the imaging of two separated nanospheres supported on different substrates with various distances between the spheres: $d = 600nm$, $d = 500nm$, $d = 400nm$ and $d = 200nm$. (a_1)-(d_1): with the enhancing TiO_2 slab on the top of glass, (a_2)-(d_2): without enhancing slab.

Optics EXPRESS

line in each subplot. For example, when the $d = 600nm$, the positions of two spheres are $x = \pm 0.791\lambda$ theoretically, which agrees well with $x_{\text{spheres}} = \pm 0.790\lambda$ in the imaging plane with the TiO_2 layer. However, the error is larger when the two spheres are only on the top of glass as presented in Fig. 6(a_2). In the same way, with the separated distance of $500nm$ (Fig. 6(b_1)), the center position is $x = \pm 0.700\lambda$ with the structure with TiO_2 slab, and the error is only 0.012λ. But in the case of glass substrate, the center positions remain the same with the decrease of separation between the spheres, as shown in Fig. 6(b_2). Therefore, the center position of the two identical spheres can also be used as a criterion to determine the localization ability as well as to judge the performance of the imaging system.

4. Conclusion

In this paper, we theoretically investigate how the resolution can be enhanced by inserting a thin dielectric slab on the top of a substrate. By using the principle of evanescent wave amplification, it is demonstrated that higher SNR, better lateral resolution and localization can be achieved when imaging subwavelength particles nearby each other. Through comparison with the case of no enhanced layer, the smallest distance between two nanospheres located on a $20nm$ thin TiO_2 layer is $d = 400nm = 0.634\lambda$, which is beyond the diffraction limit. The findings have a wide range of applications in the imaging process and can be extended in several ways, such as combining with different microscopy techniques after fabricating suitable enhancing layers for the sample [23].

Funding

China Scholarship Council; Shenzhen University.

Acknowledgements

We acknowledge Project 17FUN01 'BeCOMe' within the programme EMPIR. The EMPIR initiative is co-founded by the European Union's Horizon 2020 research and innovation programme and the EMPIR Participating Countries. We also thank to the funding from China Scholarship Council and Shenzhen University.

Disclosures

The authors declare no conflicts of interest.

References

1. E. Abbe, "Beiträge zur theorie des mikroskops und der mikroskopischen wahrnehmung," Archiv f. mikrosk. Anatomie **9**(1), 413–468 (1873).
2. M. J. Rust, M. Bates, and X. Zhuang, "Sub-diffraction-limit imaging by stochastic optical reconstruction microscopy (storm)," Nat. Methods **3**(10), 793–796 (2006).
3. E. Betzig, G. H. Patterson, R. Sougrat, O. W. Lindwasser, S. Olenych, J. S. Bonifacino, M. W. Davidson, J. Lippincott-Schwartz, and H. F. Hess, "Imaging intracellular fluorescent proteins at nanometer resolution," Science **313**(5793), 1642–1645 (2006).
4. S. T. Hess, T. P. Girirajan, and M. D. Mason, "Ultra-high resolution imaging by fluorescence photoactivation localization microscopy," Biophys. J. **91**(11), 4258–4272 (2006).
5. S. W. Hell and J. Wichmann, "Breaking the diffraction resolution limit by stimulated emission: stimulated-emission-depletion fluorescence microscopy," Opt. Lett. **19**(11), 780–782 (1994).
6. M. G. Gustafsson, "Surpassing the lateral resolution limit by a factor of two using structured illumination microscopy," J. Microsc. **198**(2), 82–87 (2000).
7. R. Dorn, S. Quabis, and G. Leuchs, "Sharper focus for a radially polarized light beam," Phys. Rev. Lett. **91**(23), 233901 (2003).
8. K. S. Youngworth and T. G. Brown, "Focusing of high numerical aperture cylindrical-vector beams," Opt. Express **7**(2), 77–87 (2000).
9. P. Meng, S. Pereira, and P. Urbach, "Confocal microscopy with a radially polarized focused beam," Opt. Express **26**(23), 29600–29613 (2018).

Optics EXPRESS

10. V. Veselago, "Electrodynamics of substances with simultaneously negative ε and μ," Usp. Fiz. Nauk **92**(7), 517 (1967).
11. J. B. Pendry, "Negative refraction makes a perfect lens," Phys. Rev. Lett. **85**(18), 3966–3969 (2000).
12. D. O. Melville and R. J. Blaikie, "Super-resolution imaging through a planar silver layer," Opt. Express **13**(6), 2127–2134 (2005).
13. S. Durant, Z. Liu, J. M. Steele, and X. Zhang, "Theory of the transmission properties of an optical far-field superlens for imaging beyond the diffraction limit," J. Opt. Soc. Am. B **23**(11), 2383–2392 (2006).
14. Z. Liu, H. Lee, Y. Xiong, C. Sun, and X. Zhang, "Far-field optical hyperlens magnifying sub-diffraction-limited objects," Science **315**(5819), 1686 (2007).
15. O. El Gawhary, N. J. Schilder, A. da Costa Assafrao, S. F. Pereira, and H. P. Urbach, "Restoration of s-polarized evanescent waves and subwavelength imaging by a single dielectric slab," New J. Phys. **14**(5), 053025 (2012).
16. C. J. Regan, D. Dominguez, L. Grave de Peralta, and A. A. Bernussi, "Far-field optical superlenses without metal," J. Appl. Phys. **113**(18), 183105 (2013).
17. S. Roy, S. Pereira, H. Urbach, X. Wei, and O. El Gawhary, "Exploiting evanescent-wave amplification for subwavelength low-contrast particle detection," Phys. Rev. A **96**(1), 013814 (2017).
18. J. D. Jackson, "Classical electrodynamics," (1999).
19. L. Novotny and B. Hecht, *Principles of nano-optics* (Cambridge University, 2012).
20. M. Paulus, P. Gay-Balmaz, and O. J. Martin, "Accurate and efficient computation of the green's tensor for stratified media," Phys. Rev. E **62**(4), 5797–5807 (2000).
21. T. Wilson, R. Juškaitis, and P. Higdon, "The imaging of dielectric point scatterers in conventional and confocal polarisation microscopes," Opt. Commun. **141**(5-6), 298–313 (1997).
22. P. Török, P. Higdon, and T. Wilson, "Theory for confocal and conventional microscopes imaging small dielectric scatterers," J. Mod. Opt. **45**(8), 1681–1698 (1998).
23. P. Meng, H. L. Pham, S. F. Pereira, and H. P. Urbach, "Demonstration of lateral resolution enhancement by focusing amplitude modulated radially polarized light in a confocal imaging system," J. Opt. **22**(4), 045605 (2020).